



CHORUS

This is the accepted manuscript made available via CHORUS. The article has been published as:

Quenches in a quasidisordered integrable lattice system: Dynamics and statistical description of observables after relaxation

Christian Gramsch and Marcos Rigol

Phys. Rev. A **86**, 053615 — Published 16 November 2012

DOI: [10.1103/PhysRevA.86.053615](https://doi.org/10.1103/PhysRevA.86.053615)

Quenches in a quasi-disordered integrable lattice system: Dynamics and statistical description of observables after relaxation

Christian Gramsch^{1,2} and Marcos Rigol^{1,3}

¹*Department of Physics, Georgetown University, Washington, DC 20057, USA*

²*Theoretical Physics III, Center for Electronic Correlations and Magnetism,
Institute of Physics, University of Augsburg, 86135 Augsburg, Germany*

³*Physics Department, The Pennsylvania State University,
104 Davey Laboratory, University Park, Pennsylvania 16802, USA*

We study the dynamics and the resulting state after relaxation in a quasi-disordered integrable lattice system after a sudden quench. Specifically, we consider hard-core bosons in an isolated one-dimensional geometry in the presence of a quasi-periodic potential whose strength is abruptly changed to take the system out of equilibrium. In the delocalized regime, we find that the relaxation dynamics of one-body observables, such as the density, the momentum distribution function, and the occupation of the natural orbitals, are, to a good approximation, power law. In that regime, we also show that observables after relaxation can be described by the generalized Gibbs ensemble, while such a description fails for the momentum distribution and the natural orbital occupations in the presence of localization. At the critical point, the relaxation dynamics is found to be slower than in the delocalized phase.

PACS numbers: 05.70.Ln, 72.15.Rn, 02.30.Ik, 05.60.Gg, 71.30.+h

I. INTRODUCTION

The nonequilibrium dynamics of isolated integrable quantum systems is constrained by a large number of conserved quantities, which generally preclude relaxation to thermal equilibrium [1–23]. This may affect current experiments that are realized in one-dimensional (1D) and quasi-1D geometries close to integrable points [24] and future technological devices. As such, this phenomenon cannot be considered as purely academic anymore. Advances in controlling and manipulating highly isolated quantum gases in low dimensions, and at very low temperatures, has made it possible to study in great detail the relaxation dynamics following an abrupt change of some of the system’s parameters [25, 26], so that questions related to the lack of thermalization can now also be addressed experimentally. For example, in Ref. [25], it was experimentally shown that the relaxation dynamics of one-dimensional atomic Bose gases do not necessarily lead to a thermal momentum distribution of the atoms.

Soon after the experimental finding in Ref. [25], it was shown in Ref. [1] that expectation values of few-body observables in isolated integrable systems after relaxation can be predicted by generalized ensembles (GGEs). GGEs are constructed by maximizing the entropy [27, 28], while satisfying constraints imposed by the constants of motion that make the system integrable. Interestingly, the mechanism that leads to thermalization in non-integrable systems, namely, eigenstate thermalization [29–32], can be generalized to the integrable case in the sense that most eigenstates that are not only close in energy but also in their distribution of conserved quantities share the same expectation values of few-body observables [3]. This allows one to understand why GGE works. The validity of GGE description after relaxation has been tested in many different integrable quantum models [1–23], and has been argued to be adequate for predicting prethermalized expectation values of observables [33–35] in non-

integrable quantum systems close to an integrable point [36].

In relation to current ultracold gases experiments (and to low-dimensional mesoscopic devices), one question that needs to be addressed is the fate of the GGE description when translational invariance is absent in the system. Numerical calculations for hard-core bosons in a box [1–3] and in the presence of a harmonic confining potential (relevant to optical lattice setups) [2, 17], have shown that the GGE indeed describes observables after relaxation. However, a recent study of quenches in the quantum Ising chain has put forward the notion that “as soon as the translational invariance is broken, the GGE fails to apply” [37]. This was supported by calculations of equal-time correlations after a quench in the presence of disorder. Since the general statement made in Ref. [37] is in contradiction with previous results [1–3, 17], specially with those in the presence of a confining potential [2, 17], here we revisit the question of whether the GGE is valid in the absence of translational invariance.

One important difference between the systems studied in Ref. [37] and those studied in Refs. [1–3] is the inclusion of disorder in the former. Even in the presence of interactions, disorder can lead to localization [38–41], and, in nonintegrable systems, localization can lead to lack of thermalization after relaxation following a quantum quench [41, 42]. The latter can be understood to follow from the failure of eigenstate thermalization in the localized regime [41]. It is then natural to expect that, in integrable systems, localization, and not necessarily the breaking of translational symmetry, may lead to a failure of the GGE. This would follow from a failure of the generalized eigenstate thermalization [3].

In order to separate the effects of breaking translational symmetry and localization in an integrable system, we study hard-core bosons in an incommensurate superlattice. This model exhibits a transition between an extended and a localized phase at a finite strength of the superlattice potential [43], and is to be contrasted with the case of uniform random disorder where localization occurs for any nonzero disorder

strength [24]. We show that in the extended phase, the GGE provides a correct description of one-body observables after relaxation, despite the lack of translational invariance. On the other hand, in the localized phase, the GGE is found to fail. At the critical point, a slower relaxation dynamics is seen to preclude the observation of stationary values of the observables for the largest system sizes. However, as long as the stationary value is reached, the GGE provides a good description of observables after relaxation at the critical point.

The exposition is organized as follows. In the next section (Sec. II), we introduce the model and observables to be studied in the remainder of the paper. We also briefly discuss the computational approach utilized in our study, as well as the ensembles that are used to compare with the results after relaxation. In Sec. III, we study the relaxation dynamics following a sudden quench in the different regimes of the model. Section IV is devoted to the comparison of observables after relaxation with the predictions of statistical ensembles, as well as a finite size scaling analysis that allows us to gain insight on the behavior in the thermodynamic limit. We also make contact with the results in Ref. [37] by studying the behavior of off-diagonal one-particle correlations. The conclusions are then presented in Sec. V.

II. MODEL, OBSERVABLES, AND ENSEMBLES

Our study is performed within the Aubry-André model [43] for hard-core bosons in a one-dimensional lattice with open boundary conditions. The Hamiltonian reads

$$\hat{H} = -t \sum_{j=1}^{L-1} (\hat{b}_j^\dagger \hat{b}_{j+1} + \text{H.c.}) + \lambda \sum_{j=1}^L \cos(2\pi\sigma j + \varphi) \hat{n}_j, \quad (1)$$

where the operator \hat{b}_j^\dagger (\hat{b}_j) creates (annihilates) a hard-core boson at site j , and $\hat{n}_j = \hat{b}_j^\dagger \hat{b}_j$ is the on-site occupation number operator. \hat{b}_j and \hat{b}_j^\dagger obey the usual bosonic commutation relations, i.e., $[\hat{b}_i, \hat{b}_j^\dagger] = \delta_{ij}$, but satisfy a constraint $\hat{b}_j^2 = \hat{b}_j^{\dagger 2} = 0$, which forbids multiple occupancy of the lattice sites. The hopping parameter is denoted by t (we set $t = 1$, $\hbar = 1$ throughout this work), L is the number of sites, and we only consider systems in which the number of particles (N) is $N = L/2$ (half filling). By selecting σ to be an irrational number, we generate a quasiperiodic potential whose strength is controlled by the parameter λ . In our study, we choose σ to be the inverse golden ratio, $\sigma = (\sqrt{5} - 1)/2$, a choice motivated by the fact that the golden mean is considered to be the most irrational number [44]. φ allows to shift the phase of the potential, and will be used later to average over different realizations in our finite systems. For most of our work, we set $\varphi = 0$.

Despite the quadratic form of Eq. (1), it cannot be directly diagonalized because of the on-site constraints forbidding multiple occupancy of the lattice sites. This can, however, be circumvented by mapping the 1D hard-core boson Hamiltonian onto a spin-1/2 chain via the Holstein-Primakoff transformation [45], and then mapping the spin-1/2 chain onto noninteracting spinless fermions [46] via the Jordan-Wigner

transformation [47]. The resulting Hamiltonian maintains the form in Eq. (1) but with the hard-core operators replaced by fermionic ones. It then follows that the spectrum, as well as thermodynamic and density related properties, are the same for hard-core bosons and non-interacting spinless fermions.

The Aubry-André model [43] is known to undergo a localization transition at a critical $\lambda_c = 2t$. For $\lambda < \lambda_c$, all single-particle states are extended, i.e., Bloch-like states. Above the critical point, single-particle states are exponentially localized with localization length $\xi = \ln(\lambda)^{-1}$ [43]. Because of the mapping above, the same holds true for hard-core bosons. This implies that the ground state of the latter undergoes a superfluid-insulating transition as $\lambda_c = 2t$ is crossed. In the localized phase, the ground state is a Bose glass [24].

In connection to optical lattice experiments, such as the ones carried out in Refs. [25, 26], we are interested in studying two different one-body observables. The on-site density $n_i = \langle \hat{n}_i \rangle$, and the momentum distribution function m_k . m_k is the diagonal part of the Fourier transform of the one-particle density matrix $\rho_{ij} = \langle \hat{b}_i^\dagger \hat{b}_j \rangle$,

$$m_k = \frac{1}{L} \sum_{i,j=0}^L e^{ik(i-j)} \rho_{ij}. \quad (2)$$

Additional information on the coherence properties of the system can be gained through the study of the natural orbitals ϕ_i^α and their occupations η_α , defined through the eigenvalue equation

$$\sum_j \rho_{ij} \phi_j^\alpha = \eta_\alpha \phi_i^\alpha. \quad (3)$$

In homogeneous periodic systems, the natural orbitals are plane waves and their occupations coincide with the momentum distribution function, so m_k and η_α give the same information about the system. However, once translational invariance is broken these two quantities become different. Out of equilibrium, they can even give apparently inconsistent results. For example, during the expansion of a hard-core boson gas its momentum distribution function becomes identical to that of noninteracting fermions, which may be taken as an indication that the system lacks coherence [48]. However, the occupation of the natural orbitals is very different from the one of fermions; many orbitals remain highly populated, which reveals the bosonic character of the out-of-equilibrium gas [48]. In addition, in higher dimensional interacting systems, if the occupation of the highest occupied natural orbital scales with the total number of particles, then one can say that the system exhibits Bose-Einstein condensation [49, 50].

In equilibrium, the properties of hard-core bosons, modeled by Eq. (1), have been studied in detail in the ground state [51, 52] and at finite temperature [53]. Here, our goal is to examine the dynamics after the system is taken out of equilibrium by a sudden change of λ ($\lambda_I \rightarrow \lambda_F$). The initial state $|\Psi_I\rangle$ is taken to be the ground state of \hat{H}_I [Eq. (1) with $\lambda = \lambda_I$] and the evolution is studied under \hat{H}_F [Eq. (1) with $\lambda = \lambda_F$]

$$|\Psi(\tau)\rangle = e^{-i\hat{H}_F \tau} |\Psi_I\rangle. \quad (4)$$

To study the time evolution of the observables introduced above, we follow a computational method based on the Bose-Fermi mapping and the use of properties of Slater determinants. This method has been explained in detail in Ref. [54], so we do not reproduce it here. It allows one to calculate each matrix element ρ_{ij} (at any given time τ) in terms of the determinant of an $(N+1) \times (N+1)$ matrix, which results from the product of two matrices with sizes $(N+1) \times L$ and $L \times (N+1)$. The computation time of the entire one-particle density matrix essentially scales as $L^2(N+1)^3$ (the matrix multiplication needs not to be done for every entry), which allows us to efficiently study the dynamics of systems of up to 1000 lattice sites.

We then contrast the time-averaged results for the observables after relaxation with the predictions of statistical mechanics. While the most relevant traditional ensemble to compare with would be the microcanonical one (because the time evolving system is isolated), we instead use the grand-canonical ensemble (GE). This is because calculations in the former scale exponentially with system size, while, in the latter, they scale power law. Within the GE, we can study very large lattices, in which we expect a good agreement between the predictions from different statistical ensembles [55]. The density matrix in the GE reads

$$\hat{\rho}_{\text{GE}} = \frac{1}{Z_{\text{GE}}} \exp\left(-\frac{\hat{H} - \mu\hat{N}}{k_B T}\right), \quad (5)$$

where k_B is the Boltzmann constant, \hat{N} is the total number operator, and Z_{GE} is the partition function

$$Z_{\text{GE}} = \text{Tr} \left[\exp\left(-\frac{\hat{H} - \mu\hat{N}}{k_B T}\right) \right]. \quad (6)$$

In order to compare the grand-canonical predictions for the observables to those obtained following the quantum dynamics, T and μ need to be chosen so that $\text{Tr}[\hat{\rho}_{\text{GE}}\hat{H}_F] = E$ and $\text{Tr}[\hat{\rho}_{\text{GE}}\hat{N}] = N$, where $E = \langle \Psi_I | \hat{H}_F | \Psi_I \rangle$ is the energy of the time evolving system after the quench, which is conserved.

In integrable hard-core bosons systems, in the absence of disorder or quasi-disorder, the grand-canonical [1–3] and microcanonical [3] descriptions have been shown to fail to predict the outcome of the relaxation dynamics for few-body observables. Instead, the GGE has been proposed to be the adequate ensemble to deal with this problem [1]. The GGE density matrix can be written as

$$\hat{\rho}_{\text{GGE}} = \frac{1}{Z_{\text{GGE}}} \exp\left(-\sum_m \lambda_m \hat{I}_m\right), \quad (7)$$

where \hat{I}_m are the conserved quantities, λ_m their corresponding Lagrange multipliers, and Z_{GGE} is the partition function

$$Z_{\text{GGE}} = \text{Tr} \left[\exp\left(-\sum_m \lambda_m \hat{I}_m\right) \right]. \quad (8)$$

The Lagrange multipliers need to be selected so that the expectation values of the conserved quantities in the GGE are the same as in the initial state, i.e., $\text{Tr}[\hat{\rho}_{\text{GGE}}\hat{I}_m] = \langle \Psi_I | \hat{I}_m | \Psi_I \rangle$. For

hard-core bosons, where the conserved quantities are taken to be the projection operators to the single-particle eigenstates of the fermionic Hamiltonian to which Eq. (1) can be mapped, the Lagrange multipliers can be written as [1]

$$\lambda_m = \ln \left(\frac{1 - \langle \Psi_I | \hat{I}_m | \Psi_I \rangle}{\langle \Psi_I | \hat{I}_m | \Psi_I \rangle} \right). \quad (9)$$

In order to calculate the expectation value of the one-particle density matrix in the grand-canonical ensemble, $\rho_{ij}^{\text{GE}} = \text{Tr} [\hat{b}_i^\dagger \hat{b}_j \hat{\rho}_{\text{GE}}]$, and in the GGE, $\rho_{ij}^{\text{GGE}} = \text{Tr} [\hat{b}_i^\dagger \hat{b}_j \hat{\rho}_{\text{GGE}}]$ (note that the GGE is also grand-canonical), we use the approach introduced in Ref. [55]. The grand-canonical calculations, similarly to the ones carried out for studying the dynamics, use the Bose-Fermi mapping and properties of Slater determinants. The computation time of the entire one-particle density matrix in this case scales as L^5 [55].

III. TIME EVOLUTION

To probe the relaxation dynamics after the quench, we calculate the normalized difference $\delta O(\tau)$ (where O stands for n , m , η) between the expectation value of observables at different times and their long-time average O_j^{avg} . $\delta O(\tau)$ is defined as

$$\delta O(\tau) = \frac{\sum_j |O_j(\tau) - O_j^{\text{avg}}|}{\sum_j O_j^{\text{avg}}}. \quad (10)$$

[Note that j is a dummy variable that stands for i (in n_i), k (in m_k), and α (in η_α).] If observables relax to stationary values, $\delta O(\tau)$ will fluctuate about a time-independent value. This value, as well as the amplitude of the time fluctuations about it, are expected to be finite for finite systems but should vanish in the thermodynamic limit. We note that O_j^{avg} is taken to be an average over a variable size time interval that contains the longest times that we have simulated. In the event that the observable has not relaxed by then, $\delta O(\tau)$ will make it evident as it will not become stationary.

In Fig. 1, we show results for $\delta O(\tau)$ in a set of quenches in which the initial state is the ground state of Eq. (1) with $\lambda_I = 0$ (i.e., a superfluid state) and λ_F is below ($\lambda_F = 1$), at ($\lambda_F = 2$), and above ($\lambda_F = 3, 4$) the localization transition. Results are presented for three different system sizes ($L = 10, 100$, and 1000 , from top to bottom in each panel). In Figs. 1(a)–1(c), one can see that all three observables in the quench terminating in the extended phase exhibit a clear relaxation dynamics in which $\delta O(\tau)$ decreases as time passes, and then fluctuates about a finite time-independent value. Both, the finite time-independent value and the amplitude of the fluctuations, are seen to decrease with increasing system size.

The quench towards the critical point ($\lambda_F = 2$) [Figs. 1(d)–1(f)] exhibits a different dynamics. As the system size increases beyond 100 sites, the three observables considered here do not reach a clear stationary value during the times studied (up to $\tau = 10^6$ for n_i and $\tau = 5.37 \times 10^4$ for m_k and η_α). This can be understood as the critical point is known to

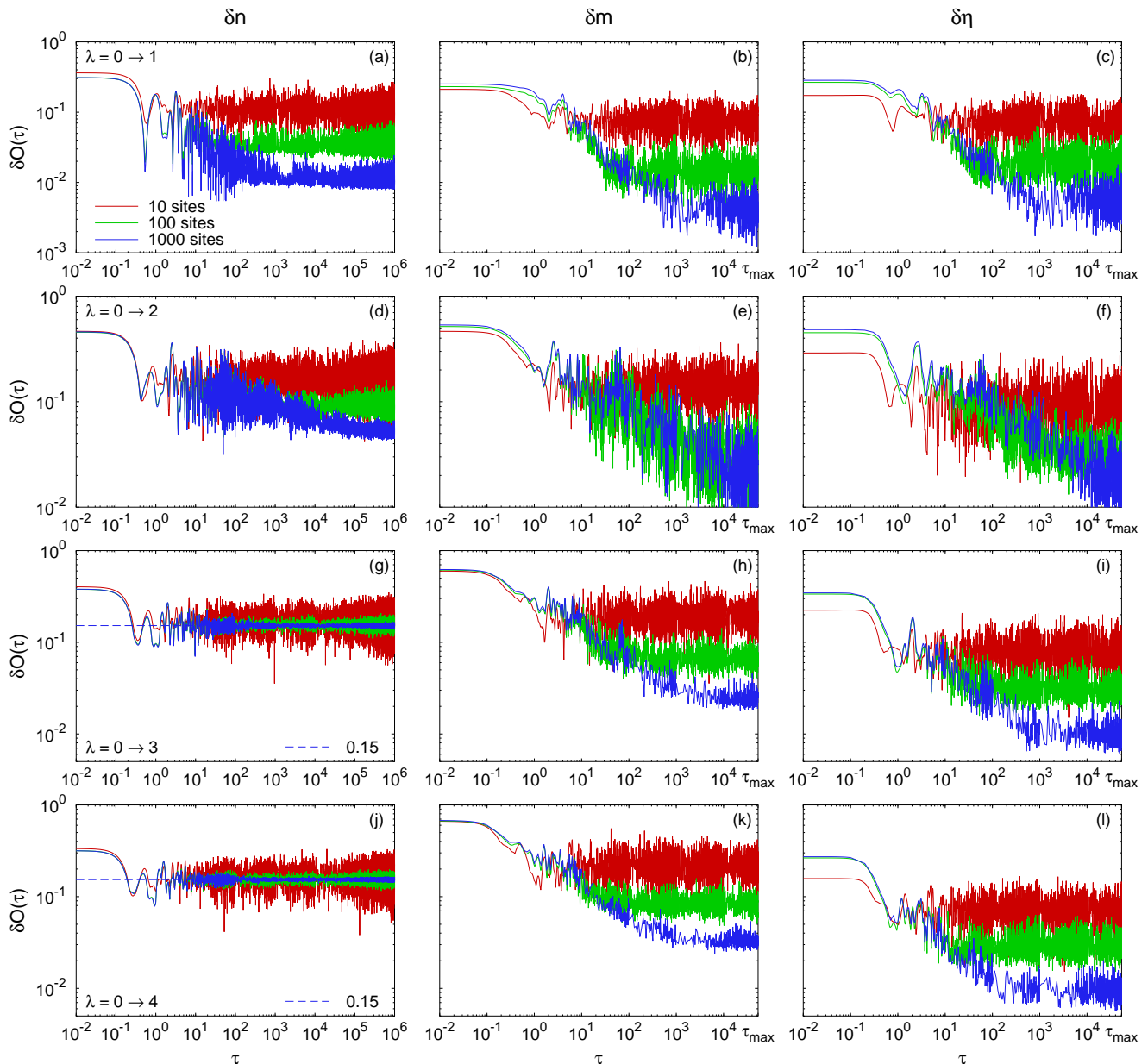


FIG. 1: (Color online) Relaxation dynamics of n_i , m_k , and η_α as they approach the long-time average in a quench $\lambda_I = 0 \rightarrow \lambda_F = 1$ (a)–(c), $\lambda_I = 0 \rightarrow \lambda_F = 2$ (d)–(f), $\lambda_I = 0 \rightarrow \lambda_F = 3$ (g)–(i), and $\lambda_I = 0 \rightarrow \lambda_F = 4$ (j)–(l), for systems with 10, 100, and 1000 lattice sites (from top to bottom in each panel). The time averages are computed as follows: since n_i is computationally less expensive than m_k and η_α , for that observable we simulated longer times and averaged over 9000 steps with $\tau \in [10^5, 10^6]$ for all lattice sizes. For m_k and η_α , we averaged over 900 steps with $\tau \in [10^4, 10^5]$ for $L = 10$ and $L = 100$, and over 437 steps for $L = 1000$ with $\tau \in [10^4, 5.37 \times 10^4]$ (in the plots, $\tau_{\max} = 5.37 \times 10^4$).

be very special. The single particle spectrum becomes a Cantor set (the bands acquire zero measure), and the gaps form a devil's staircase [56]. Such a peculiar spectrum seems to render dephasing ineffective in these systems. Our finding implies that, at the critical point, stationary values of the observables may be more difficult to observe experimentally.

Finally, the quench towards the localized regime [Figs. 1(g)–1(i) for $\lambda_F = 3$ and Figs. 1(j)–1(l) for $\lambda_F = 4$] does lead to stationary values for m_k , and η_α . Note that m_k , and η_α exhibit dynamics that are qualitative similar to the

one observed in the quench $\lambda_I = 0 \rightarrow \lambda_F = 1$, namely, the stationary values of δm and $\delta \eta$ (and the fluctuations about them) decrease with increasing system size. n_i , on the other hand, exhibits a different behavior. Because of localization in real space, δn becomes lattice size independent, i.e., it remains finite in the thermodynamic limit. In that case, the only effect that increasing L has is to reduce the amplitude of the time fluctuations of δn about the stationary value.

We have also studied quenches starting from different initial states that are eigenstates of Eq. (1), and even from the

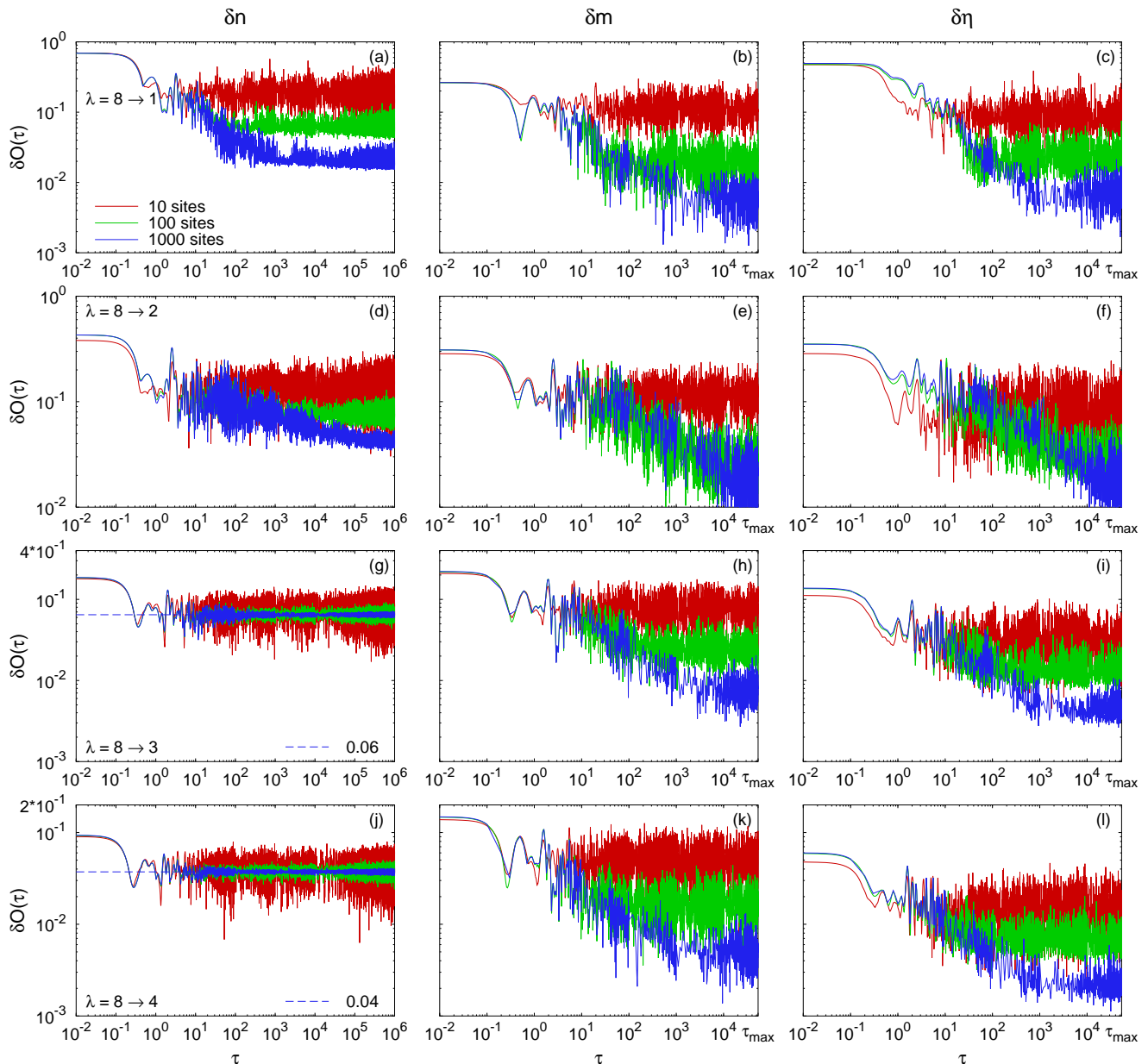


FIG. 2: (Color online) Same as Fig. 1 but for quenches from $\lambda_I = 8$, i.e., from deep inside the Bose-glass phase.

ground of commensurate superlattices such as the ones studied in Refs. [2, 18, 21], finding a qualitatively similar dynamics to the one depicted in Fig. 1. As an example of a different initial state, in Fig. 2, we report results in which the quenches start from the ground state of Hamiltonian (1) deep inside the Bose-glass phase ($\lambda_I = 8$). Figure 2 shows that the dynamics is indeed very similar to the one reported in Fig. 1. The only apparent difference is that for quenches within the Bose-glass phase ($\lambda_I = 8 \rightarrow \lambda_F = 3$ and $\lambda_I = 8 \rightarrow \lambda_F = 4$), the stationary value of δn is smaller than in the quenches from the superfluid phase to the Bose-glass phase ($\lambda_I = 0 \rightarrow \lambda_F = 3$ and $\lambda_I = 0 \rightarrow \lambda_F = 4$). For the former, we find $\delta n^{8 \rightarrow 3}(\infty) \approx 0.06$ and $\delta n^{8 \rightarrow 4}(\infty) \approx 0.04$ while for the latter $\delta n^{0 \rightarrow 3}(\infty) \approx \delta n^{0 \rightarrow 4}(\infty) \approx 0.15$. This is understandable as

$\delta n(0)$ is already smaller in quenches starting in the Bose-glass phase than in those starting in the superfluid phase.

Approach to the stationary values

In a recent numerical study of the relaxation dynamics of a disordered nonintegrable fermionic system with short-range interactions and random long-range hopping, it was found that, in the extended phase, observables exhibit a power-law approach to their thermal expectation values [41]. Power-law like relaxation dynamics was also seen in recent optical lattice experiments with a clean system in a one-dimensional geometry [26]. These results are to be contrasted with the expo-

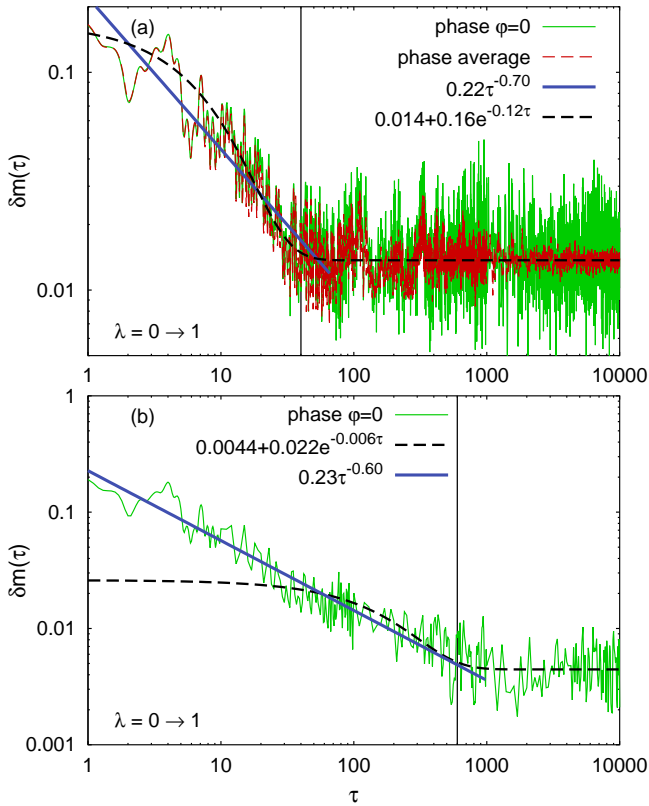


FIG. 3: (Color online) (a) δm_k vs τ for $\varphi = 0$, as well as after averaging over 1000 random values of φ (uniformly distributed in $[0, 2\pi]$), in systems with 100 lattice sites. The fits to power-law and exponential behavior were done over the interval $\tau \in [1, 40]$ (a vertical line marks $\tau = 40$), which contains 1200 data points. (b) δm_k vs τ for $\varphi = 0$ in a system with 1000 lattice sites. The fits to power-law and exponential behavior were done over the interval $\tau \in [1, 600]$ (a vertical line marks $\tau = 600$), which contains 230 data points.

ponential approach expected in generic nonintegrable systems. Since both studies [26, 41] were limited to small lattice sizes, and no extensive scaling analysis could be performed, it is not clear how these findings are affected by finite size effects.

The dynamics depicted in Figs. 1 and 2 for three system sizes, which are a decade away from each other, provide a clearer picture of the role of finite size effects. We indeed find indications of power-law relaxation, as it is apparent in the plots that the time interval over which a power-law like behavior is seen increases with system size. We explicitly show this in Fig. 3, where we compare the relaxation process for systems with 100 and 1000 lattice sites. In the former [Fig. 3(a)], both, power-law and exponential decay provide a reasonable fit to the data. In the latter [Fig. 3(b)], where power-law behavior is apparent for about three decades, a fit to an exponential decay is clearly inconsistent with the data. Hence, our results provide another example of a system in which, whenever relaxation takes place, the relaxation dynamics is power law. To what extent power-law like relaxation is generic to the dynamics of isolated quantum systems, specially nonintegrable ones, is a topic that deserves further attention.

Since we are dealing with finite lattice sizes with open boundary conditions, we have also studied the effect that averaging over different phases φ [see Eq. (1)] has on our results. A typical outcome of such an average is depicted in Fig. 3(a), for 1000 different values of φ distributed uniformly in $[0, 2\pi]$. The average over different phases can be seen to reduce time fluctuations after relaxation, but leaves the results for the approach to the stationary value almost unaffected.

Another important question to be answered, which is of special interest to current experiments with ultracold gases, is how long it takes for observables to reach the stationary values. Given the strong indications found above that the relaxation dynamics is power law, the times at which stationary values are attained will be determined by how $\delta n(\infty)$, $\delta m(\infty)$ and $\delta \eta(\infty)$ (here, “ ∞ ” should be understood as long-time after relaxation) scale with system size. In Fig. 4, we show

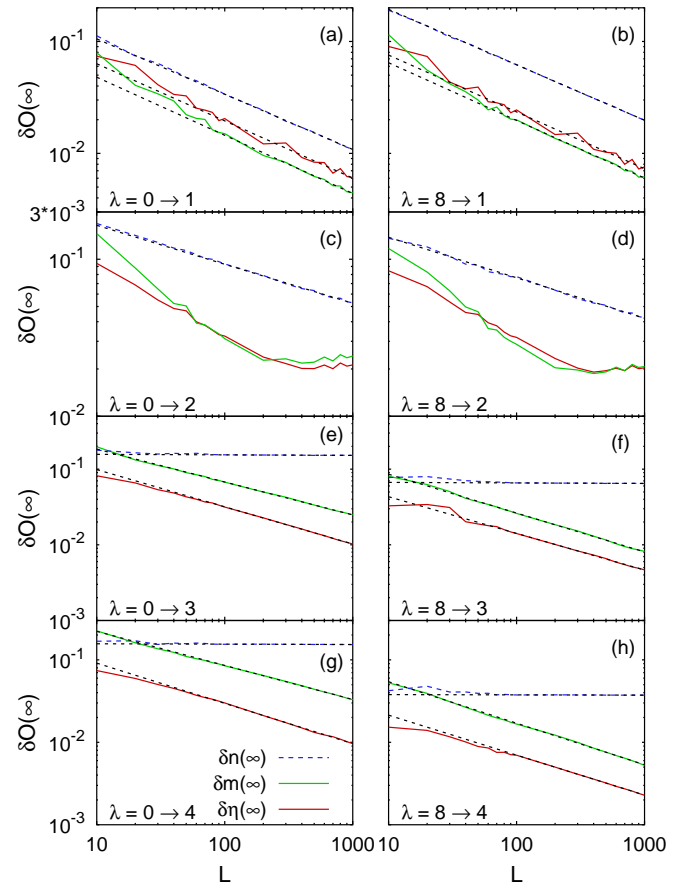


FIG. 4: (Color online) Finite size scaling of $\delta n(\infty)$, $\delta m(\infty)$ and $\delta \eta(\infty)$ for the quenches studied in Figs. 1 and 2. The dashed lines are power-law fits leading to $\delta n(\infty) \propto L^{-0.49}$, $\delta m(\infty) \propto L^{-0.52}$ and $\delta \eta(\infty) \propto L^{-0.51}$ in (a), $\delta n(\infty) \propto L^{-0.50}$, $\delta m(\infty) \propto L^{-0.52}$ and $\delta \eta(\infty) \propto L^{-0.51}$ in (b), $\delta n(\infty) \propto L^{-0.25}$ in (c), $\delta n(\infty) \propto L^{-0.26}$ in (d), $\delta n(\infty) \propto L^{-0.01}$, $\delta m(\infty) \propto L^{-0.43}$ and $\delta \eta(\infty) \propto L^{-0.49}$ in (e), $\delta n(\infty) \propto L^{-0.01}$, $\delta m(\infty) \propto L^{-0.51}$ and $\delta \eta(\infty) \propto L^{-0.48}$ in (f), $\delta n(\infty) \propto L^0$, $\delta m(\infty) \propto L^{-0.41}$ and $\delta \eta(\infty) \propto L^{-0.49}$ in (g), $\delta n(\infty) \propto L^0$, $\delta m(\infty) \propto L^{-0.50}$ and $\delta \eta(\infty) \propto L^{-0.48}$ in (h). The power-law fits were done using the data for systems between 100 and 1000 lattice sites (eleven data points).

the scaling of those quantities in the quenches analyzed in Figs. 1 and 2. Figures 1(a), 1(b), and 1(e)–1(f) show that, away from the critical point, the scaling of $\delta m(\infty)$ and $\delta \eta(\infty)$ is close to $1/\sqrt{L}$, and a similar scaling is seen for $\delta n(\infty)$ in quenches to the extended phase [Figs. 1(a) and 1(b)]. Such a scaling has been proven to provide a bound for the normalized time variance of observables that are quadratic in Fermi operators in noninteracting fermion models [57], but we find it to be also applicable to more general observables in integrable systems. As discussed before, in quenches to the localized regime, $\delta n(\infty)$ becomes independent of system size. Also, the slow relaxation dynamics of m and η at the critical point precludes the observation of a clear scaling for $\delta m(\infty)$ and $\delta \eta(\infty)$ [Figs. 1(c) and 1(d)], while the scaling of $\delta n(\infty)$ is close to $1/L^{1/4}$. The scaling of $\delta n(\infty)$ at the critical point and in the localized regime violate the bound proven in Ref. [57].

A power-law approach of $\delta n(\tau)$, $\delta m(\tau)$ and $\delta \eta(\tau)$ to the stationary values, together with a power-law scaling of $\delta n(\infty)$, $\delta m(\infty)$ and $\delta \eta(\infty)$ with system size, implies that the time at which stationary values are attained increases as a power law with system size. This means that measuring densities and momentum distribution functions in experiments is advantageous with respect to directly measuring two-point correlation functions. After relaxation, the values of the latter have been shown to be exponentially small with the distance between the points [2, 23] and, as such, the time it takes for those correlations to relax to the stationary values increases exponentially with the distance between the points [23].

IV. DESCRIPTION AFTER RELAXATION

After discussing the relaxation dynamics, we focus on the description of the observables after relaxation. In generic (non-integrable) quantum systems, one expects the dynamics to lead to thermalization, namely, to expectation values of observables that are equal to those of a system in thermal equilibrium. Because of thermodynamic universality, this is expected to be true whenever the isolated system and its thermal equilibrium counterpart share the same mean energy and number of particles [29–32], independently of the initial state in the former.

In Fig. 5, we show results for n_i , m_k , and η_α for quenches from initial states with $\lambda_I = 0$, and $\lambda_F = 1$ and 4. For all quantities, we report their values in the initial state, the long-time averages, and within the GE and the GGE. The plots for the density in the initial state [Figs. 5(a) and 5(d)] make evident that, despite the presence of open boundary conditions, at $\tau = 0$ the density is constant throughout the system. This is because of the particle-hole symmetry of the model. After the quench, this is not true anymore and the density becomes time dependent and inhomogeneous. Remarkably, the time-averaged result for the density after relaxation and the predictions of the GGE are almost indistinguishable from each other for $\lambda_F = 1$ in Fig. 5(a) and $\lambda_F = 4$ in Fig. 5(d). The predictions of the GE are different from the outcome of the relaxation dynamics in both quenches.

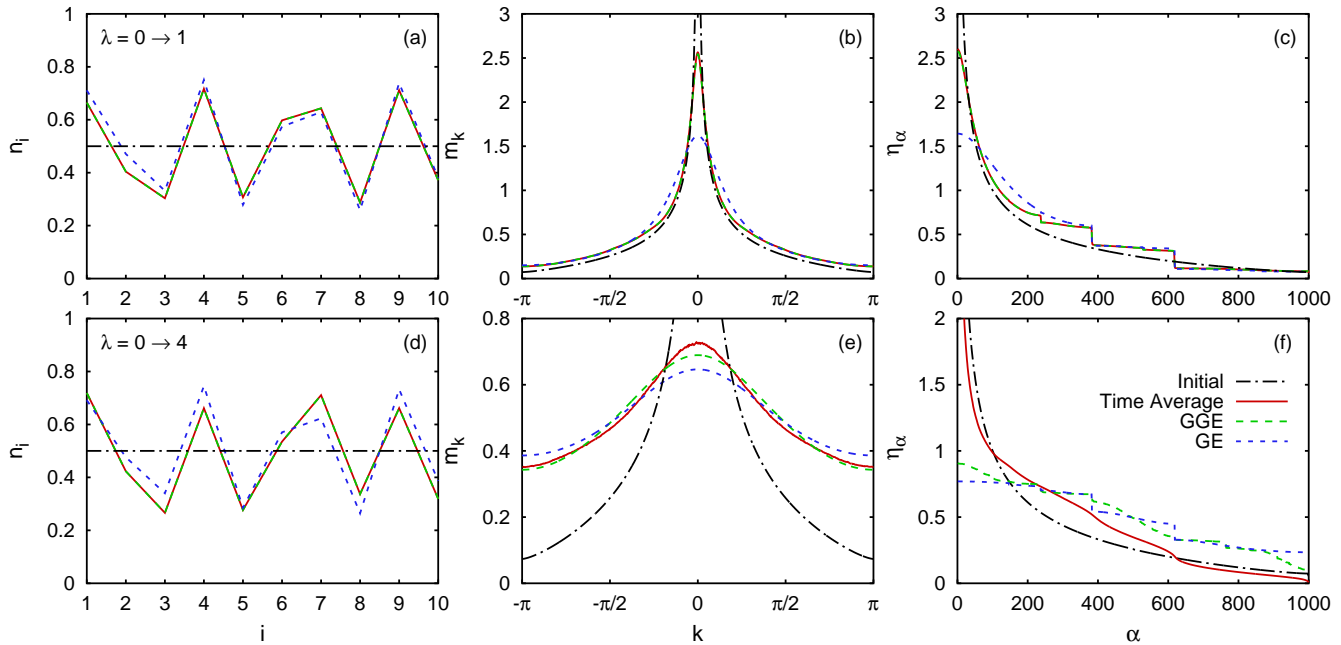


FIG. 5: (Color online) Density in the first 10 sites [(a),(d)], momentum distribution function [(b),(e)], and natural orbital occupations [(c),(f)] for quenches in which the initial state is the superfluid ground state of a system with $\lambda_I = 0$ while $\lambda_F = 1$ [(a)–(c)], $\lambda_F = 4$ [(d)–(f)], and for $L = 1000$. We present results for the observables in the initial state, the long-time average (calculated between $\tau = 10^5$ to $\tau = 10^6$ for n_i (9000 steps), and between $\tau = 10^4$ and $\tau = 5.37 \times 10^4$ (437 steps) for m_k and η_α , see the caption of Fig. 1), as well as within the GE and the GGE. Note that, except $\delta n(\infty)$ for $\lambda_F = 4$, $\delta n(\infty)$, $\delta m(\infty)$ and $\delta \eta(\infty)$ are very small for $L = 1000$ (see Fig. 4). In addition, we have checked that all time averages are well converged.

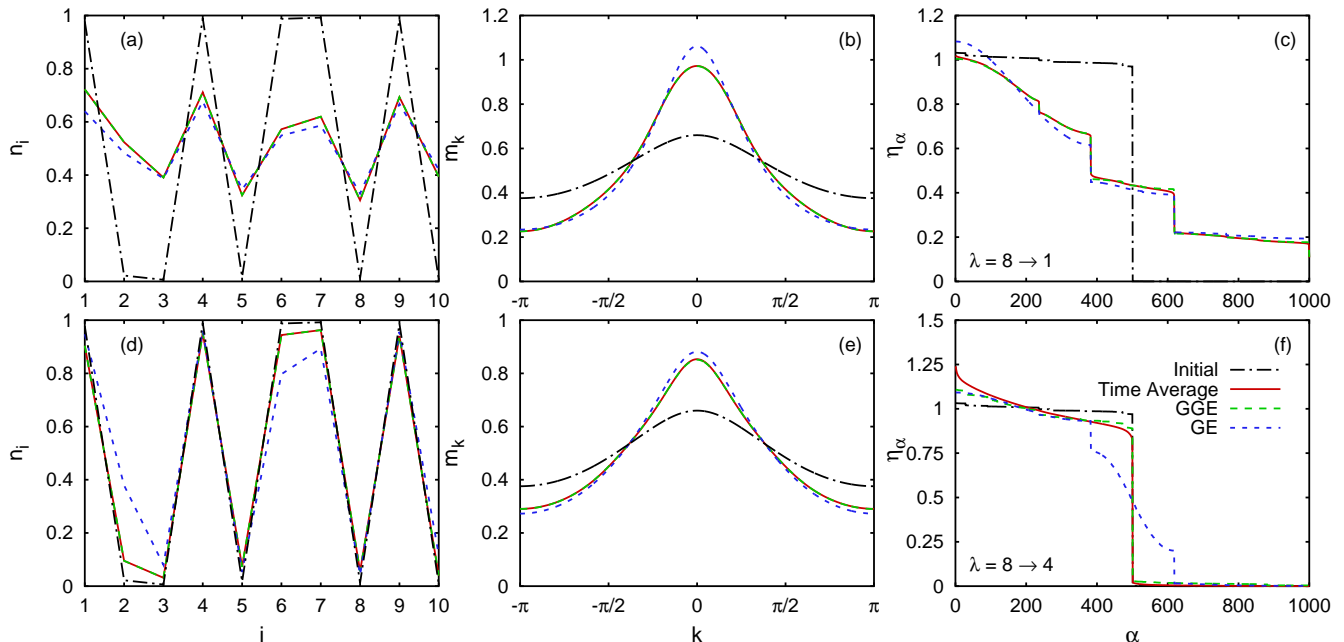


FIG. 6: (Color online) Same as Fig. 5 but for quenches from $\lambda_I = 8$, i.e., from deep inside the Bose-glass phase.

Two other identifying properties of the initial state, which signal the existence of off-diagonal quasi-long range correlations, are the presence of a sharp peak in m_k at $k = 0$ [Figs. 5(b) and 5(e)] and in η_α at $\alpha = 0$ [Figs. 5(c) and 5(f)]. The quenches can be seen to lead to a dramatic decrease of the height of those peaks after relaxation, which is similar to the effect of finite temperature in equilibrium systems [55]. For m_k and η_α , a stark contrast can be observed between the results obtained for the quench $\lambda_I = 0 \rightarrow \lambda_F = 1$ and those obtained for the quench $\lambda_I = 0 \rightarrow \lambda_F = 4$. While, in the former, the time-averaged results and the GGE predictions are almost indistinguishable from each other, the same is not true for the latter. This suggests that the transition to localization plays an important role in the description after relaxation. In addition, the thermal values for both observables in the GE are clearly different from the results after relaxation.

Qualitatively, we have obtained a very similar picture to the one gained through Fig. 5, for what happens after relaxation in the extended and localized regimes, for a wide range of different initial states. Among those, we considered ground states and excited states of hard-core boson Hamiltonians in the form of Eq. (1) but with different local potentials, including period-two superlattices [2, 18, 21]. In Fig. 6, we show results for the case in which the initial state is the ground state of Eq. (1) with $\lambda = 8$. In contrast to the case with $\lambda_I = 0$, for $\lambda_I = 8$ the initial state is deep into the Bose-glass phase where the density is inhomogeneous [Figs. 6(a) and 6(d)] and the system lacks coherence. The latter is reflected by the almost flat initial momentum distribution [Figs. 6(b) and 6(e)]. Localization in this regime is revealed by the natural orbital occupations [Figs. 6(c) and 6(f)], which is nearly one for the first 500 orbitals (there are 500 particles in the system), i.e.,

the bosons in this many-body system can be seen as single particles localized within a few sites. This picture is confirmed by the form of the natural orbital wave functions (not shown).

After the relaxation dynamics following the quenches $\lambda_I = 8 \rightarrow \lambda_F = 1$ and $\lambda_I = 8 \rightarrow \lambda_F = 4$, one can infer from Fig. 6 [panels (b), (c), (e), and (f)] that one-particle correlations are enhanced from the ones in the initial state. This follows as the height of the zero momentum occupations increases, the zero momentum peaks become narrower, and the occupation of the lowest natural orbitals depart from one. This is the very different from what happens in the quenches $\lambda_I = 0 \rightarrow \lambda_F \neq 0$ depicted in Fig. 5, where one-particle correlations are reduced. Despite of this contrast, we find that the GGE results are almost indistinguishable from the time-average ones for all observables in quenches $\lambda_I = 8 \rightarrow \lambda_F = 1$, while for quenches $\lambda_I = 8 \rightarrow \lambda_F = 4$ only the density and m_k are accurately described by the GGE. In the latter quench, the GGE fails to describe the natural orbital occupations, pointing once again towards the role of localization.

Scaling with system size

Even more important than the actual differences seen in Figs. 5 and 6 between the long-time averages and the predictions of statistical ensembles (GE and GGE) is how those differences scale with increasing system size ($L = 1000$ in those figures). One could imagine, for example, that while the differences between the time averages and the GE are large for finite systems they may disappear in the thermodynamic limit. Another possibility is that the differences between the time averages and the GGE are small for the quenches and sys-

tem sizes studied here but they may not vanish in the thermodynamic limit, which would invalidate the GGE description for thermodynamic systems. Cases in which integrable systems seemed to behave thermally, but failed to exhibit the required scaling with system size, were recently studied in Refs. [18, 21].

In order to study the scaling of the discrepancies between the time averages and the statistical predictions, we compute the normalized differences ΔO between the long-time average of the observables O_i^{avg} and the ensemble predictions $O_i^{\text{GGE/GE}}$

$$\Delta O^{\text{GGE/GE}} = \frac{\sum_j |O_j^{\text{avg}} - O_j^{\text{GGE/GE}}|}{\sum_j O_j}. \quad (11)$$

Note that O stands for n , m , and η , and j is a dummy variable that stands for i , k , and α , respectively. This quantity is defined in the same spirit as δO in Eq. (10).

In Fig. 7, we show the scaling of $\Delta m^{\text{GGE/GE}}$ and $\Delta \eta^{\text{GGE/GE}}$ for the quenches studied in Figs. 1 and 2. Apparent differences can be seen between the scalings when λ_F lies in the ex-

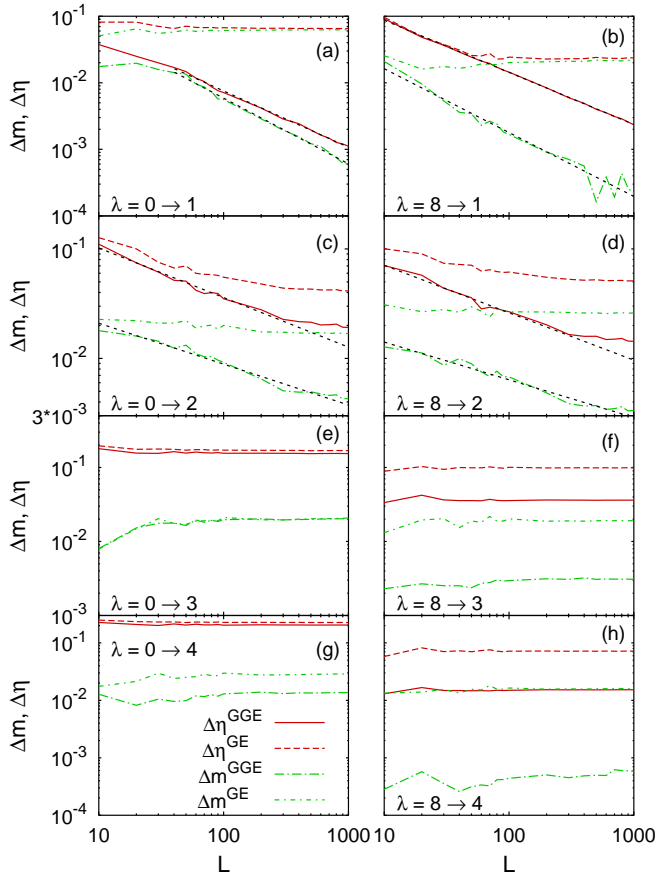


FIG. 7: (Color online) Finite size scaling of $\Delta m^{\text{GGE/GE}}$ and $\Delta \eta^{\text{GGE/GE}}$ for the quenches studied in Figs. 1 and 2. The dashes lines in (a)–(e) are power-law fits leading to $\Delta m^{\text{GGE}} \propto L^{-0.99}$ and $\Delta \eta^{\text{GGE}} \propto L^{-0.85}$ in (a), and $\Delta m^{\text{GGE}} \propto L^{-0.96}$ and $\Delta \eta^{\text{GGE}} \propto L^{-0.78}$ in (b). Up to 100 sites, the time average was taken over 900 steps with $\tau \in [10^4, 10^5]$. For all other system sizes, the time average was taken over 437 steps with $\tau \in [10^4, 5.37 \times 10^4]$.

tended, critical, and localized regimes. Different initial states, on the other hand, lead to qualitatively similar behavior of $\Delta O^{\text{GGE/GE}}$, i.e., λ_F is the parameter that determines how the outcome of the relaxation dynamics compares to the predictions of statistical ensembles.

In quenches terminating in the extended phase [$\lambda_F = 1$, Figs. 7(a) and 7(b)], one can see that Δm^{GGE} and $\Delta \eta^{\text{GGE}}$ exhibit a power-law decrease with increasing system size. The small oscillations in Δm^{GGE} , seen in Fig. 7(b) for the largest system sizes, are due to the small values of this quantity. They depend on the exact time intervals and number of time steps used in the time averages. Hence, such oscillations are an artifact of our numerical calculations and are not expected to be present if one takes the infinite time averages used in previous works [3, 31], which are not available here. Δm^{GE} and $\Delta \eta^{\text{GE}}$, on the other hand, exhibit a clear saturation to finite values with increasing system size. From these scalings, we conclude that the GGE correctly describes m_k and η_α after relaxation, despite the absence of translational invariance and the presence of disorder. On the contrary, the GE fails to describe those observables, which makes evident that these systems do not thermalize in the traditional sense.

Quenches terminating at the critical point [$\lambda_F = 2$, Figs. 7(c) and 7(d)], and except for the largest system sizes, display a behavior that is qualitatively similar to the one seen in quenches to the extended regime. Namely, they exhibit a power-law like decrease of Δm^{GGE} and $\Delta \eta^{\text{GGE}}$ with increasing system size. However, a tendency towards saturation can also be seen in the differences for the largest system sizes. These can be attributed to the failure of the observables to relax to stationary values for the times considered here [see Figs. 1 and 2]. Hence, as long as relaxation is achieved, the GGE provides a good description of observables also at the critical point. The GE, on the other hand, fails to describe m_k and η_α (as it does in the extended regime).

The quenches to the localized phase [$\lambda_F = 3$, Figs. 7(e) and 7(f), and $\lambda_F = 4$, Figs. 7(g) and 7(h)] exhibit a very different scaling of Δm^{GGE} and $\Delta \eta^{\text{GGE}}$ from the one observed in those to the extended regime and the critical point. One can see in the corresponding panels in Fig. 7 that, for $\lambda_F = 3$ and $\lambda_F = 4$, Δm^{GGE} and $\Delta \eta^{\text{GGE}}$ are almost constant with increasing system size, the same way (up to an offset) that Δm^{GE} and $\Delta \eta^{\text{GE}}$ are. This makes evident that the GGE description breaks down in the localized phase, in a similar way that standard statistical ensembles fail, in general, to describe integrable systems after relaxation. We should note, however, that the GGE predictions are closer to the long-time averages than the ones provided by the GE, as expected given the larger number of constraints imposed in the former ensemble.

We have also studied the scaling of the differences Δn^{GGE} and Δn^{GE} for all parameter regimes depicted in Fig. 7. We find that Δn^{GE} behaves similarly to Δm^{GE} and $\Delta \eta^{\text{GE}}$, i.e., it saturates to finite values with increasing system size. On the contrary, Δn^{GGE} exhibits a qualitatively different behavior from Δm^{GGE} and $\Delta \eta^{\text{GGE}}$. Independently of λ_F , we find that Δn^{GGE} is very small and almost size independent. This is particularly interesting because n_i is a property that is shared by hard-core bosons and noninteracting fermions. Given the very small val-

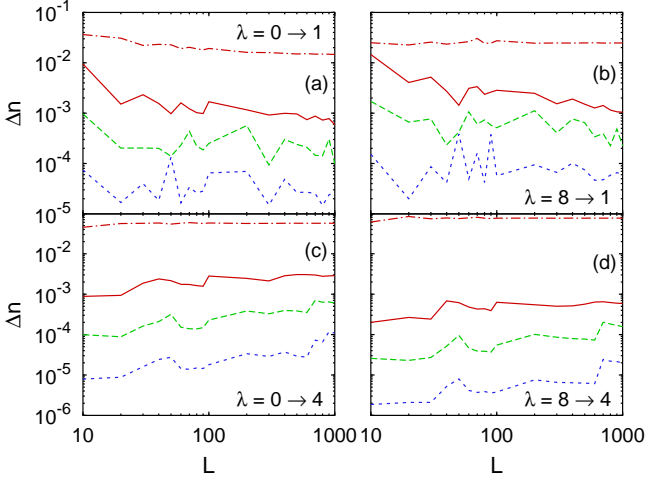


FIG. 8: (Color online) Scaling of Δn^{GGE} and Δn^{GE} with increasing system size. Results for Δn^{GGE} are reported for time averages calculated using different numbers of time steps. Since the differences Δn^{GGE} are very small, the number of time steps used in the average determine the result. The continuous (red) line shows an average over 99 steps with $\tau \in [9.9 \times 10^5, 10^6]$, the dashed (green) line an average over 990 steps with $\tau \in [9 \times 10^5, 10^6]$, and the dotted (blue) line an average over 9900 steps with $\tau \in [10^4, 10^6]$. The dashed-dotted (red) line shows Δn^{GE} for an average over 9900 steps.

ues we obtain for Δn^{GGE} , this quantity is strongly affected by the width of the time interval used to calculate the time averages as well as by the number of time steps used. Evidence of this dependence is presented in Fig. 8 for quenches with $\lambda_F = 1$ and $\lambda_F = 4$ (the results for other values of λ_F are qualitatively similar).

From the results reported in Fig. 8, we conclude that the GGE provides the correct description for the density distribution after relaxation following a quench both in the extended and localized regimes. While the former may have been expected, the latter is somehow surprising in view of the behavior of m_k and η_α in the localized regime (the GGE fails to describe the latter two). However, the generalized eigenstate thermalization discussed in Ref. [3] can help one understand why the GGE works in the localized phase when the observable is the density. For $\lambda_F > 2$, the eigenstates of the Hamiltonian are localized within a number of sites (l) that depends on λ_F . The conserved quantities are the occupations of those eigenstates, and those occupations are nothing but added on-site occupations within l sites. This implies that eigenstates of the Hamiltonian with similar expectation values of the conserved quantities should also have similar distributions of the on-site occupations. Hence, the generalized eigenstate thermalization, which is expected to be valid for n_i , m_k , and η_α in the extended regime, may also valid for n_i in the localized regime. From this, it would then follow that, in the localized regime, the GGE provides the correct description for n_i after relaxation. Note that this argument works equally well for other integrable disordered systems that exhibit real-space localization.

One-particle correlations

The three observables we have studied throughout this work provide complementary information about one-particle correlations, some of which are currently accessible in ultracold gases experiments (n_i and m_k). In order to conclude our study, and to make contact with the discussion in Ref. [37], we also directly analyze the behavior of one-particle correlations. Note that ρ_{ij} is a complex Hermitian matrix, and this is why n_i , m_k , and η_α are all real quantities.

In Fig. 9, we show how the absolute value of ρ_{ij} decays when i is fixed to be the central site in the lattice ($i = L/2$) and j moves towards the boundaries. Results are presented for two different initial states for quenches towards the extended, critical, and localized regimes, for different times (as well as for the time average), and within the GGE and the GE. The behavior of ρ_{ij} in the initial state (in equilibrium ρ_{ij} is real) reflects the nature of the ground state in the extended and localized phases. In the former, one-particle correlations exhibit a power-law decay ($\rho_{ij} \propto 1/\sqrt{|i-j|}$), no matter the value of λ , while in the latter they decay exponentially [52].

The quenches towards the extended phase [Figs. 9(a) and 9(b)] exhibit clear similarities no matter the value of λ_F . We find that: (i) $|\rho_{ij}|$ is very similar, but not the same, for $\tau = 100$, $\tau = 1000$, and the time average. (ii) The time average and the GGE results show an excellent agreement with each other. (iii) ρ_{ij} exhibits a faster, and featureless, exponential decay in

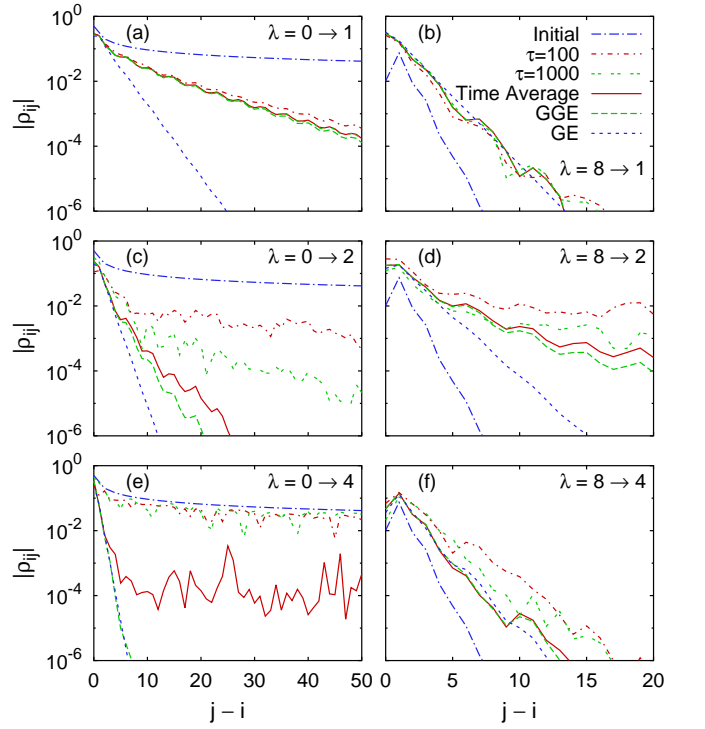


FIG. 9: (Color online) Decay of the absolute value of ρ_{ij} for $i = 500$ and $j \geq 500$ in a system with $L = 1000$. The time average was taken over 437 steps with $\tau \in [10^4, 5.37 \times 10^4]$. The results depicted are the absolute values after taking those time averages [$\rho_{ij}(\tau)$ is complex].

the GE. This is all consistent with our conclusion that the GGE provides the adequate description of one-particle observables after relaxation, while the GE fails to do so in this regime.

Figures 9(c) and 9(d) depict results for quenches to the critical point. In this case, due to the slow relaxation dynamics discussed before, the values of $|\rho_{ij}|$ at different times differ from each other and from the time average. The time-averaged results can be seen to be closest to the GGE prediction and are clearly distinct from those in the GE. Calculating the time averages for later times (not depicted) do improve the agreement between those averages and the GGE predictions, revealing a picture similar to the one obtained for quenches to the extended phase in Figs. 9(a) and 9(b).

Results for quenches to the localized phase are presented in Figs. 9(e) and 9(f). Once again, $|\rho_{ij}|$ at different times differ from each other and from the time average. The latter is also different (although quite close for the quench $\lambda_I = 8 \rightarrow \lambda_F = 4$) to the GGE predictions. This is compatible with our previous findings that the GGE fails to describe m_k and η_α after relaxation in this regime. Further understanding of the behavior seen for these quenches can be gained by analyzing the case in which $\lambda_F \rightarrow \infty$, so that Hamiltonian (1) can be written as $\hat{H} = \sum_j \epsilon_j \hat{n}_j$, where ϵ_j is the local chemical potential in each site. It then follows that

$$\rho_{ij}(\tau) = \langle \Psi(\tau) | b_i^\dagger b_j | \Psi(\tau) \rangle \approx \rho_{ij}(0) e^{i(\epsilon_i - \epsilon_j)\tau} \quad (12)$$

which means that if one quenches deep into the localized phase, $|\rho_{ij}(\tau)| \approx \rho_{ij}(0)$, i.e., correlations present in the initial state are preserved, similarly to what we see in Fig. 9(e).

We note that our results in Figs. 9(e) and 9(f) are similar to the ones reported in Fig. 3 in Ref. [37] for two-point correlations of the order parameter. However, the contrast between Figs. 9(e) and 9(f) and Figs. 9(a) and 9(b) make evident that the failure of the GGE in disordered systems is a consequence of localization and not of the breaking of translational symmetry. Our results also make clear the importance of computing time averages, for complex quantities such as ρ_{ij} , before comparing with the predictions of the GGE.

V. SUMMARY

In this work, we studied the dynamics and description after relaxation of hard-core bosons in one-dimensional lattices after a sudden change of the strength of an additional quasi-periodic potential. This model features two distinct regimes, an extended regime for weak quasi-periodic potentials and a localized regime for strong quasi-periodic poten-

tials. Our analysis has shown that the approach of observables towards their time-independent values after relaxation is close to power law. For the finite system sizes studied, all observables reach their time-independent values within the considered time scales. The sole exception were the quenches towards the critical point, where the dynamics were found to be slower and time-independent values of the observables were not reached for the largest lattices. We have argued that, in most of the cases analyzed, the times required for the observables to reach their stationary values increase power law with the system size

We further compared the long-time average of observables with statistical descriptions provided by the GE and the GGE. The GE failed to describe all observables after relaxation in the quenches considered, as expected since these systems are integrable. The GGE, on the other hand, was found to provide a good description of observables after relaxation in the extended phase, and at the critical point, whenever observables became time independent (up to vanishingly small fluctuations). The scaling behavior in these two cases suggests that, in the thermodynamic limit, the GGE results are identical to those after relaxation. On the contrary, in the localized regime, we have found that the GGE fails to describe observables that depend on nonlocal correlations (such as m_k and η_α) after relaxation, and that this picture does not change with changing system size. The density, on the other hand, was found to be well described by the GGE in all regimes.

From the outcome of this study, as well as from the results in Refs. [1–3, 17], we conclude that localization, and not the breaking of translational symmetry as proposed in Ref. [37], can lead to the breakdown of the GGE description. Our work also poses the question of whether modifying the GGE by using a different set of conserved quantities (here we used the occupation of the single particle eigenstates of the noninteracting fermionic system to which hard-core bosons can be mapped), or adding further conserved quantities, would allow one to describe time averages of observables in the localized regime. Recent work on finding optimal sets of conserved quantities may shed light on these questions [58].

Acknowledgments

This work was supported by NSF under Grant No. OCI-0904597 and by the Office of Naval Research. We thank E. Khatami and K. He for helpful discussions and comments on the manuscript.

[1] M. Rigol, V. Dunjko, V. Yurovsky, and M. Olshanii, Phys. Rev. Lett. **98**, 050405 (2007).
 [2] M. Rigol, A. Muramatsu, and M. Olshanii, Phys. Rev. A **74**, 053616 (2006).
 [3] A. C. Cassidy, C. W. Clark, and M. Rigol, Phys. Rev. Lett. **106**, 140405 (2011).

[4] M. A. Cazalilla, Phys. Rev. Lett. **97**, 156403 (2006).
 [5] P. Calabrese and J. Cardy, J. Stat. Mech. p. P06008 (2007).
 [6] M. Cramer, C. M. Dawson, J. Eisert, and T. J. Osborne, Phys. Rev. Lett. **100**, 030602 (2008).
 [7] T. Barthel and U. Schollwöck, Phys. Rev. Lett. **100**, 100601 (2008).

- [8] M. Eckstein and M. Kollar, *Phys. Rev. Lett.* **100**, 120404 (2008).
- [9] M. Kollar and M. Eckstein, *Phys. Rev. A* **78**, 013626 (2008).
- [10] A. Iucci and M. A. Cazalilla, *Phys. Rev. A* **80**, 063619 (2009).
- [11] D. Rossini, A. Silva, G. Mussardo, and G. E. Santoro, *Phys. Rev. Lett.* **102**, 127204 (2009).
- [12] D. Rossini, S. Suzuki, G. Mussardo, G. E. Santoro, and A. Silva, *Phys. Rev. B* **82**, 144302 (2010).
- [13] D. Fioretto and G. Mussardo, *New J. Phys.* **12**, 055015 (2010).
- [14] A. Iucci and M. A. Cazalilla, *New J. Phys.* **12**, 055019 (2010).
- [15] J. Mossel and J.-S. Caux, *New J. Phys.* **12**, 055028 (2010).
- [16] P. Calabrese, F. H. L. Essler, and M. Fagotti, *Phys. Rev. Lett.* **106**, 227203 (2011).
- [17] M. A. Cazalilla, A. Iucci, and M.-C. Chung, *Phys. Rev. E* **85**, 011133 (2012).
- [18] M. Rigol and M. Fitzpatrick, *Phys. Rev. A* **84**, 033640 (2011).
- [19] M.-C. Chung, A. Iucci, and M. A. Cazalilla, arXiv:1203.0121 (2012).
- [20] M. Kormos, A. Shashi, Y.-Z. Chou, and A. Imambekov, arXiv:1204.3889 (2012).
- [21] K. He and M. Rigol, *Phys. Rev. A* **85**, 063609 (2012).
- [22] P. Calabrese, F. H. L. Essler, and M. Fagotti, *J. Stat. Mech.* p. P07016 (2012).
- [23] P. Calabrese, F. H. L. Essler, and M. Fagotti, *J. Stat. Mech.* p. P07022 (2012).
- [24] M. A. Cazalilla, R. Citro, T. Giamarchi, E. Orignac, and M. Rigol, *Rev. Mod. Phys.* **83**, 1405 (2011).
- [25] T. Kinoshita, T. Wenger, and D. Weiss, *Nature* **440**, 900 (2006).
- [26] S. Trotzky, Y.-A. Chen, A. Flesch, I. P. McCulloch, U. Schollwöck, J. Eisert, and I. Bloch, *Nature Phys.* **8**, 325 (2012).
- [27] E. T. Jaynes, *Phys. Rev.* **106**, 620 (1957).
- [28] E. T. Jaynes, *Phys. Rev.* **108**, 171 (1957).
- [29] J. M. Deutsch, *Phys. Rev. A* **43**, 2046 (1991).
- [30] M. Srednicki, *Phys. Rev. E* **50**, 888 (1994).
- [31] M. Rigol, V. Dunjko, and M. Olshanii, *Nature* **452**, 854 (2008).
- [32] M. Rigol and M. Srednicki, *Phys. Rev. Lett.* **108**, 110601 (2012).
- [33] J. Berges, S. Borsányi, and C. Wetterich, *Phys. Rev. Lett.* **93**, 142002 (2004).
- [34] M. Moeckel and S. Kehrein, *Phys. Rev. Lett.* **100**, 175702 (2008).
- [35] M. Moeckel and S. Kehrein, *Ann. Phys.* **324**, 2146 (2009).
- [36] M. Kollar, F. Wolf, and M. Eckstein, *Phys. Rev. B* **84**, 054304 (2011).
- [37] T. Caneva, E. Canovi, D. Rossini, G. E. Santoro, and A. Silva, *J. Stat. Mech.* p. P07015 (2011).
- [38] D. M. Basko, I. L. Aleiner, and B. L. Altshuler, *Ann. Phys.* **321**, 1126 (2006).
- [39] V. Oganesyan and D. A. Huse, *Phys. Rev. B* **75**, 155111 (2007).
- [40] A. Pal and D. A. Huse, *Phys. Rev. B* **82**, 174411 (2010).
- [41] E. Khatami, M. Rigol, A. Relaño, and A. M. García-García, *Phys. Rev. E* **85**, 050102(R) (2012).
- [42] C. Gogolin, M. P. Müller, and J. Eisert, *Phys. Rev. Lett.* **106**, 040401 (2011).
- [43] S. Aubry and G. André, *Ann. Israel Phys. Soc.* **3**, 133 (1980).
- [44] J. B. Sokoloff, *Phys. Rep.* **126**, 189 (1985).
- [45] T. Holstein and H. Primakoff, *Phys. Rev.* **58**, 1098 (1940).
- [46] E. Lieb, T. Shultz, and D. Mattis, *Ann. Phys. (NY)* **16**, 406 (1961).
- [47] P. Jordan and E. Wigner, *Z. Phys.* **47**, 631 (1928).
- [48] M. Rigol and A. Muramatsu, *Phys. Rev. Lett.* **94**, 240403 (2005).
- [49] O. Penrose and L. Onsager, *Phys. Rev.* **104**, 576 (1956).
- [50] A. J. Leggett, *Rev. Mod. Phys.* **73**, 307 (2001).
- [51] A. M. Rey, I. I. Satija, and C. W. Clark, *Phys. Rev. A* **73**, 063610 (2006).
- [52] K. He, I. I. Satija, C. W. Clark, A. M. Rey, and M. Rigol, *Phys. Rev. A* **85**, 013617 (2012).
- [53] N. Nesi and A. Iucci, *Phys. Rev. A* **84**, 063614 (2011).
- [54] M. Rigol and A. Muramatsu, *Mod. Phys. Lett.* **19**, 861 (2005).
- [55] M. Rigol, *Phys. Rev. A* **72**, 063607 (2005).
- [56] P. Harper, *Proc. Phys. Soc. London A* **68**, 874 (1955).
- [57] L. C. Venuti and P. Zanardi, arXiv:1208.1121 (2012).
- [58] M. Olshanii, arXiv:1208.0582 (2012).